View metadata, citation and similar papers at core.ac.uk
brought to you by CORE
provided by CiteSeerX

Proceedings of IMECE2002
ASME International Mechanical Engineering Congress & Exposition
November 17–22, 2002, New Orleans, Louisiana

IMECE2002-39116

EFFECTS OF RADIAL IMMERSION AND CUTTING DIRECTION ON CHATTER INSTABILITY IN END-MILLING

Philip V. Bayly
Washington University, St. Louis, MO
Tony L. Schmitz
NIST, Gaithersburg, MD
Gabor Stepan
Budapest University of Technology and Economics

Brian P. Mann
Washington University, St. Louis, MO
David A. Peters
Washington University, St. Louis, MO
Tamas Insperger
Budapest University of Technology and Economics

ABSTRACT

Low radial immersion end-milling involves intermittent cutting. If the tool is flexible, its motion in both the x- and y-directions affects the chip load and cutting forces, leading to chatter instability under certain conditions. Interrupted cutting complicates stability analysis by imposing sharp periodic variations in the dynamic model. Stability predictions for the 2-DOF model differ significantly from prior 1-DOF models of interrupted cutting. In this paper stability boundaries of the 2-DOF milling process are determined by three techniques and compared: (1) a frequency-domain technique developed by Altintas and Budak (1995); (2) a method based on time finite element analysis; and (3) the statistical variance of periodic 1/tooth samples in a time-marching simulation. Each method has advantages in different situations. The frequency-domain technique is fastest, and is accurate except at very low radial immersions. The temporal FEA method is significantly more efficient than time-marching simulation, and provides accurate stability predictions at small radial immersions. The variance estimate is a robust and versatile measure of stability for experimental tests as well as simulation. Experimental up-milling and down-milling tests, in a simple model with varying cutting directions, agree well with theory.

1 INTRODUCTION

Milling is a metal cutting process in which the cutting tool intermittently enters and leaves the workpiece, unlike turning, in which the tool is always in contact. In both milling and turning chatter is an important instability that limits metal removal rate. Tlusty and co-workers (Tlusty, 1962, e.g.) and Tobias (1965) developed frequency-domain methods for stability analysis of continuous cutting. These methods have been used widely to determine exact stability boundaries for turning, and approximate stability boundaries for milling. Significant improvements were made by Minis and Yanushevsky (1993) and Altintas and Budak (1995). In particular, Altintas and Budak (1995) provide a complete frequency-domain algorithm for end-milling that accounts for x- and y-deflection of the tool, and uses a truncated Fourier series to approximate the periodic entry and exit of the tool from the cut. With a single Fourier series term, this method provides accurate stability predictions except for cuts with very low radial immersion where a small fraction of time is spent in the cut.

Davies et al. (2000, 2001) analyzed the limiting case of extremely low radial immersion milling. A 1-DOF model of interrupted cutting was cast in the form of a discrete "map" in the time domain; the stability of the map was used to predict the existence of additional stability regions, and to characterize the transitions to instability. Their results for the 1-DOF model were confirmed independently by Corpus and Endres (2000) using Floquet theory and experiment, and by Stépan and Insperger (2000); these methods were not restricted to infinitesimal times in the cut. Bayly et al. (2001) extended the approach of Davies and co-workers by the use of time finite element analysis (TFEA). This approach also led to stability analysis of a discrete map, as in the method of Davies et al. (2000, 2001), but the requirement of small time in the cut was relaxed. Analytical and experimental results were obtained for a 1-DOF system (Bayly et al., 2001).

In this paper we extend to 2-DOF and higher the TFEA method presented in Bayly et al. (2001). The extension to 2-DOF is important because a realistic model of milling must account for both x- and y-deflections. Behavior predicted by a 1-DOF model may not be found in a 2-DOF model. Furthermore, the 2-DOF formulation requires that all equations be expressed in a matrix-vector form that can be further extended to an arbitrary number of degrees of freedom. TFEA stability predictions are compared to frequency-domain

Copyright © 2002 by ASME

Downloaded From: https://proceedings.asmedigitalcollection.asme.org on 06/29/2019 Terms of Use: http://www.asme.org/about-asme/terms-of-use

predictions obtained by the method of Altintas and Budak (1995), and to the results of time-marching simulation. Stability of the simulation was determined from the variance of 1/tooth samples; an approach recently developed by Schmitz and co-workers (2001a, b, c).

A 1-DOF experimental system was used to confirm some the theoretical predictions obtained by TFEA. In particular, incorporation of the cutter rotation angle leads to significant differences in the stability charts for interrupted up-milling and down-milling. Once/tooth sampling of the vibration time series clearly differentiates stable and unstable behavior.

2 MODEL AND STABILITY ANALYSIS

2.1 Cutting forces and tool dynamics

2.1.1 Two-DOF model

A basic model of 2-DOF milling with a flexible tool is illustrated in Figure 1. A single mode in each of two perpendicular directions is accounted for, and the part is assumed to be rigid. The tool is not required to be symmetric. For the system of Figure 1, the equations of motion are:

$$m_x\ddot{x} + c_x\dot{x} + k_x x = F_x = \sum_{n=1}^{N} F_{cn}\cos\theta_n(t) - F_{tn}\sin\theta_n(t) \quad (1a)$$

$$m_y\ddot{y} + c_y\dot{y} + k_y y = F_y = \sum_{n=1}^{N} -F_{cn}\sin\theta_n(t) - F_{tn}\cos\theta_n(t) \quad (1b)$$

where N is the number of teeth, F_{cn} is the "cutting" or tangential component of cutting force, and F_{tn} is the "thrust" or radial component. The angle of each tooth is simply the tool rotation angle plus the pitch angle of the respective tooth: $\theta_n = \theta + \phi_n$. An approximate linear relationship between chip area and cutting force is commonly used:

$$F_{cn} = k_c b d_n \qquad F_{tn} = k_t b d_n \quad (2a,b)$$

where *b* is the axial depth of cut and d_n is the chip thickness: a function of feed, tool rotation, tool deflection and tool deflection at the time of previous tooth passage, $\vec{x}(t-T)$.

$$d_n = d_0(\theta_n) + [x(t) - x(t-T)]\sin\theta_n(t) + [y(t) - y(t-T)]\cos\theta_n(t), \quad \text{tooth } n \text{ in contact} \quad (3a)$$

$$d_n = 0, \quad \text{tooth } n \text{ not in contact} \quad (3b)$$

This model can be compactly represented by the matrix equation

$$M\ddot{\vec{x}} + C\dot{\vec{x}} + K\vec{x} = K_c(\theta)b[\vec{x} - \vec{x}(t-T)] + b\vec{f}_0(\theta), \quad (4)$$

where the displacement vector and dynamic matrices corresponding to Figure 1 are:

$$\vec{x} = \begin{Bmatrix} x \\ y \end{Bmatrix}, \quad M = \begin{bmatrix} m_x & 0 \\ 0 & m_y \end{bmatrix}, \quad C = \begin{bmatrix} c_x & 0 \\ 0 & c_y \end{bmatrix}, \quad K = \begin{bmatrix} k_x & 0 \\ 0 & k_y \end{bmatrix} \quad (5)$$

The "cutting stiffness matrix" and force vector incorporate a switching function $g(\theta_n)$ to account for entry and exit of each tooth. Both terms also include trigonometric dependencies due to tool rotation.

$$K_c(\theta) = \sum_{n=1}^{N} g(\theta_n)\begin{bmatrix} k_c sc - k_t s^2 & k_c c^2 - k_t sc \\ k_c s^2 - k_t sc & -k_c sc - k_t c^2 \end{bmatrix},$$

$$\vec{f}_0(\theta) = \sum_{n=1}^{N} g(\theta_n) d_0(\theta_n)\begin{bmatrix} k_c c - k_t s \\ -k_c s - k_t c \end{bmatrix} \quad (6a,b)$$

$$g(\theta_n) = 1 \qquad \theta_{entry} < \theta_n < \theta_{exit} \quad (7a)$$

$$g(\theta_n) = 0 \qquad \theta_n < \theta_{entry},\ \theta_n > \theta_{exit} \quad (7b)$$

Here $c = \cos\theta_n(t)$, $s = \sin\theta_n(t)$ are used to abbreviate the equations.

2.1.2 Single-DOF cutting with cutter rotation angle

If one degree of freedom is constrained, or is much stiffer dynamically than the other degree of freedom, the system can be analyzed as a single-degree-of-freedom (1-DOF) system. Considering only the x-direction, the second column and row of Equation 4 can be deleted, and the resulting equation of motion becomes:

$$m\ddot{x} + c\dot{x} + kx = -K_s(\theta)b[x(t) - x(t-T)] - f_o(\theta)b \quad (8)$$

where

$$K_s(\theta) = \sum_{p=1}^{N} g_p(t)(K_t\cos\theta_p + K_n\sin\theta_p)\sin\theta_p \quad (9a)$$

$$f_o(\theta) = \sum_{p=1}^{N} g_p(t)(K_t\cos\theta_p + K_n\sin\theta_p)h\sin\theta_p \quad (9b)$$

This 1-DOF model differs from the 1-DOF model analyzed in Bayly et al. (2001) because of the dependence of terms $K_s(\theta)$ and $f_o(\theta)$ on the cutter rotation angle θ. This allows investigation of differences between up-milling and down-milling in a 1-DOF model. This model was studied because a reliable 1-DOF experimental test-bed was available for experimental validation.

Copyright © 2002 by ASME

Downloaded From: https://proceedings.asmedigitalcollection.asme.org on 06/29/2019 Terms of Use: http://www.asme.org/about-asme/terms-of-use

2.2 Stability analysis

2.2.1 TFEA analysis of a 2-DOF system

In low-radial immersion milling (or for any cut less than a full slot, with a 2-fluted tool), the tool switches between cutting and not cutting. When out of the cut, the free vibration of the tool can be described exactly, in closed form. When the tool is in the cut, there is no exact solution to the equation of motion because of the time-delayed terms. However, we can break up the time in the cut into multiple elements and approximate the vector displacement on a single element as a linear combination of polynomial trial functions. The derivation below parallels that shown in Bayly et al. (2001). The displacement on the jth element is:

$$\vec{x}(t) = \sum_{i=1}^{4} \vec{a}_{ji}^{\,n} \phi_i(\tau) \tag{10}$$

The "local" time on this jth element, $\tau = t - nT - \sum_{k=1}^{j-1} t_k$, is defined so that $0 < \tau < t_j$. The length of the kth element is t_k and the trial functions $\phi_i(\tau)$ are the cubic Hermite polynomials

$$\phi_1(\tau) = 1 - 3\left(\frac{\tau}{t_j}\right)^2 + 2\left(\frac{\tau}{t_j}\right)^3, \tag{11a}$$

$$\phi_2(\tau) = t_j\left\{\left(\frac{\tau}{t_j}\right) - 2\left(\frac{\tau}{t_j}\right)^2 + \left(\frac{\tau}{t_j}\right)^3\right\}, \tag{11b}$$

$$\phi_3(\tau) = 3\left(\frac{\tau}{t_j}\right)^2 - 2\left(\frac{\tau}{t_j}\right)^3, \tag{11c}$$

$$\phi_4(\tau) = t_j\left\{-\left(\frac{\tau}{t_j}\right)^2 + \left(\frac{\tau}{t_j}\right)^3\right\}. \tag{11d}$$

These functions are particularly useful because of their end conditions:

$$\phi_1(0) = 1, \dot{\phi}_1(0) = 0, \phi_1(t_j) = 0, \dot{\phi}_1(t_j) = 0 \tag{12a}$$

$$\phi_2(0) = 0, \dot{\phi}_2(0) = 1, \phi_2(t_j) = 0, \dot{\phi}_2(t_j) = 0, \tag{12b}$$

$$\phi_3(0) = 0, \dot{\phi}_3(0) = 0, \phi_3(t_j) = 1, \dot{\phi}_3(t_j) = 0, \tag{12c}$$

$$\phi_4(0) = 0, \dot{\phi}_4(0) = 0, \phi_4(t_j) = 0, \dot{\phi}_4(t_j) = 1. \tag{12d}$$

The end conditions allow the coefficients of the polynomials to correspond directly to the initial and final values of displacement and velocity for each element.

Initial conditions:

$$\vec{x}(t_{0j}^n) = \vec{a}_{j1}^{\,n}, \qquad \vec{v}(t_{0j}^n) = \vec{a}_{j2}^{\,n}, \tag{13a}$$

Final conditions:

$$\vec{x}(t_{1j}^n) = \vec{a}_{j3}^{\,n}, \qquad \vec{v}(t_{1j}^n) = \vec{a}_{j4}^{\,n}, \tag{13b}$$

where:

$$t_{0j}^n = \left(nT + \sum_{k=1}^{j-1} t_k\right); \qquad t_{1j}^n = \left(nT + \sum_{k=1}^{j} t_k\right). \tag{13c}$$

For the assumed form of the solution, on the jth element the time-delayed displacement is

$$\vec{x}(t-T) = \sum_{i=1}^{4} \vec{a}_{ji}^{\,n-1} \phi_i(\tau) \tag{14}$$

and the velocity and acceleration on the jth element are given by

$$\dot{\vec{x}}(t) = \sum_{i=1}^{4} \vec{a}_{ji}^{\,n} \dot{\phi}_i, \qquad \ddot{\vec{x}}(t) = \sum_{i=1}^{4} \vec{a}_{ji}^{\,n} \ddot{\phi}_i. \tag{15}$$

Substitution of the assumed solution into the equation of motion leads to a non-zero error. If the error is "weighted" by a set of test functions, $\psi_p(\tau), p = 1,2$ (Hou and Peters, 1994) and the integral of the weighted error is set to zero, we obtain two vector equations per element. The test functions are chosen to be the functions that provide a measure of average error and linearly increasing error: $\psi_1(\tau) = 1$ (constant) and $\psi_2(\tau) = \tau / t_j - 1/2$ (linear). The two equations are, for p=1,2:

$$\begin{aligned}\int_0^{t_j} \left\{ M\left(\sum_{i=1}^{4} \vec{a}_{ji}^{\,n} \ddot{\phi}_i \psi_p\right) + C\left(\sum_{i=1}^{4} \vec{a}_{ji}^{\,n} \dot{\phi}_i \psi_p\right) + K\left(\sum_{i=1}^{4} \vec{a}_{ji}^{\,n} \phi_i \psi_p\right)\right\} d\tau \\ - \int_0^{t_j} b\left\{ \vec{f}_0 + K_c\left(\sum_{i=1}^{4} \vec{a}_{ji}^{\,n} \phi_i\right) - K_c\left(\sum_{i=1}^{4} \vec{a}_{ji}^{\,n-1} \phi_i\right)\right\} \psi_p d\tau = 0,\end{aligned} \tag{16}$$

Evaluation of the definite integrals leads to two algebraic equations that are linear in the coefficients of the trial functions. These equations can be written as a single matrix equation for the jth element.

$$\begin{bmatrix} N_{11} & N_{12} & N_{13} & N_{14} \\ N_{21} & N_{22} & N_{23} & N_{24} \end{bmatrix} \begin{Bmatrix} \vec{a}_{j1} \\ \vec{a}_{j2} \\ \vec{a}_{j3} \\ \vec{a}_{j4} \end{Bmatrix}^n = \begin{Bmatrix} \vec{C}_1 \\ \vec{C}_2 \end{Bmatrix} + \begin{bmatrix} P_{11} & P_{12} & P_{13} & P_{14} \\ P_{21} & P_{22} & P_{23} & P_{24} \end{bmatrix} \begin{Bmatrix} \vec{a}_{j1} \\ \vec{a}_{j2} \\ \vec{a}_{j3} \\ \vec{a}_{j4} \end{Bmatrix}^{n-1} \tag{17}$$

Copyright © 2002 by ASME

Downloaded From: https://proceedings.asmedigitalcollection.asme.org on 06/29/2019 Terms of Use: http://www.asme.org/about-asme/terms-of-use

where

$$N_{pi} = \int_0^{t_j} \left\{ M\ddot{\phi}_i + C\dot{\phi}_i + (K + bK_c)\phi_i \right\} \psi_p \, d\tau \,, \quad \text{(2x2)} \quad \text{(18a)}$$

$$\vec{C}_p = \int_0^{t_j} b\vec{f}_0 \psi_p \, d\tau \,, \quad \text{(2x1)} \quad \text{(18b)}$$

$$P_{pi} = \int_0^{t_j} bK_c \phi_i \psi_p \, d\tau \,. \quad \text{(2x2)} \quad \text{(18c)}$$

In the previous expressions, note that the cutting forces and stiffness matrices depend on the angle of tool rotation, which depends on time. So in the above integrals, $K_c = K_c(\theta(\tau))$ and $\vec{f}_0 = \vec{f}_0(\theta(\tau))$.

While the tool is in the cut, the position and velocity at the end of one element are equal to the position and velocity at the beginning of the next element.

$$\begin{Bmatrix} \vec{a}_{j1} \\ \vec{a}_{j2} \end{Bmatrix}^n = \begin{Bmatrix} \vec{a}_{(j-1)3} \\ \vec{a}_{(j-1)4} \end{Bmatrix}^n . \quad (19)$$

The initial and final conditions during free vibration are related by a state transition matrix, using the coefficients $\vec{a}_{ji}$ to specify position and velocity:

$$\begin{Bmatrix} \vec{a}_{11} \\ \vec{a}_{12} \end{Bmatrix}^n = \left[e^{At_f} \right] \begin{Bmatrix} \vec{a}_{E3} \\ \vec{a}_{E4} \end{Bmatrix}^{n-1} , \quad (20a)$$

where

$$A = -\begin{bmatrix} 0 & M \\ I & 0 \end{bmatrix}^{-1} \begin{bmatrix} K & C \\ 0 & -I \end{bmatrix} . \quad (20b)$$

and where E is the total number of finite elements in the cut. Finally, Equations 17-20 can be rearranged to obtain the coefficients of the assumed solution in terms of (i) the coefficients at the time of the previous tooth passage, and (ii) the periodic nominal cutting force. The following expression is for the case when the number of elements, E=3.

$$\begin{bmatrix} \mathbf{I} & \mathbf{0} & \mathbf{0} & \mathbf{0} \\ \mathbf{N_1} & \mathbf{N_2} & \mathbf{0} & \mathbf{0} \\ \mathbf{0} & \mathbf{N_1} & \mathbf{N_2} & \mathbf{0} \\ \mathbf{0} & \mathbf{0} & \mathbf{N_1} & \mathbf{N_2} \end{bmatrix} \begin{Bmatrix} \begin{bmatrix} \vec{a}_{11} \\ \vec{a}_{12} \end{bmatrix} \\ \begin{bmatrix} \vec{a}_{21} \\ \vec{a}_{22} \end{bmatrix} \\ \begin{bmatrix} \vec{a}_{31} \\ \vec{a}_{32} \end{bmatrix} \\ \begin{bmatrix} \vec{a}_{33} \\ \vec{a}_{34} \end{bmatrix} \end{Bmatrix}^n =$$

$$\begin{bmatrix} \mathbf{0} & \mathbf{0} & \mathbf{0} & e^{At_f} \\ \mathbf{P_1} & \mathbf{P_2} & \mathbf{0} & \mathbf{0} \\ \mathbf{0} & \mathbf{P_1} & \mathbf{P_2} & \mathbf{0} \\ \mathbf{0} & \mathbf{0} & \mathbf{P_1} & \mathbf{P_2} \end{bmatrix} \begin{Bmatrix} \begin{bmatrix} \vec{a}_{11} \\ \vec{a}_{12} \end{bmatrix} \\ \begin{bmatrix} \vec{a}_{21} \\ \vec{a}_{22} \end{bmatrix} \\ \begin{bmatrix} \vec{a}_{31} \\ \vec{a}_{32} \end{bmatrix} \\ \begin{bmatrix} \vec{a}_{33} \\ \vec{a}_{34} \end{bmatrix} \end{Bmatrix}^{n-1} + \begin{Bmatrix} \begin{bmatrix} 0 \\ 0 \end{bmatrix} \\ \begin{bmatrix} \vec{C}_1 \\ \vec{C}_2 \end{bmatrix} \\ \begin{bmatrix} \vec{C}_1 \\ \vec{C}_2 \end{bmatrix} \\ \begin{bmatrix} \vec{C}_1 \\ \vec{C}_2 \end{bmatrix} \end{Bmatrix} \quad (21)$$

where the sub-matrices are:

$$\mathbf{N_1} = \begin{bmatrix} N_{11} & N_{12} \\ N_{21} & N_{22} \end{bmatrix}, \quad \mathbf{N}_2 = \begin{bmatrix} N_{13} & N_{14} \\ N_{23} & N_{24} \end{bmatrix}, \quad \text{(4x4)} \quad \text{(22a)}$$

$$\mathbf{P_1} = \begin{bmatrix} P_{11} & P_{12} \\ P_{21} & P_{22} \end{bmatrix}, \quad \mathbf{P}_2 = \begin{bmatrix} P_{13} & P_{14} \\ P_{23} & P_{24} \end{bmatrix}. \quad \text{(4x4)} \quad \text{(22b)}$$

For larger numbers of elements, E, the global matrices, of dimensions $(4E+4)\times(4E+4)$ are analogous to the matrices of Equation 21.

Equation 21 describes a linear discrete dynamical system, or map that can be written as

$$\mathbf{A}\vec{a}_n = \mathbf{B}\vec{a}_{n-1} + \vec{C} \,. \quad (23)$$

or

$$\vec{a}_n = \mathbf{Q}\vec{a}_{n-1} + \vec{D} \quad (24)$$

Stability is determined from the eigenvalues of the matrix **Q**. Eigenvalues of magnitude greater than 1 indicate instability.

Note that the effect of vibration on geometric part accuracy (Schmitz and Ziegert, 1999) can be analyzed by this technique as well. Surface location error is specified by the value of the coefficient corresponding to displacement normal to the surface at the time the tooth leaves the cut in down-milling (or enters the cut in up-milling). In the steady state,

$$\vec{a}_n = \vec{a}_{n-1} = \vec{a}^* \quad (25)$$

Copyright © 2002 by ASME

Downloaded From: https://proceedings.asmedigitalcollection.asme.org on 06/29/2019 Terms of Use: http://www.asme.org/about-asme/terms-of-use

and thus the steady-state vector of coefficients is

$$\vec{a}^* = (I - \mathbf{Q})^{-1}\vec{D} \tag{26}$$

Since the matrix $\mathbf{Q}$ and vector $\vec{D}$ can be computed exactly for each speed and depth of cut, the steady-state displacement can be found, and can be used to specify surface location error as a function of machining process parameters.

2.2.2 Generalization to multiple modes

Suppose that multiple modes are involved in both the x- and y- directions. Let the modes be normalized to unity amplitude at the tool tip, so that:

$$x(t) = \sum_{r=1}^{R} \eta_r \ , \quad y(t) = \sum_{r=1}^{R} \xi_r \ . \tag{27}$$

The x- and y-modes are governed by

$$m_{rx}\ddot{\eta}_r + c_{rx}\dot{\eta}_r + k_{rx}\eta_r = F_x = \sum_{n=1}^{N} F_{cn}\cos\theta_n(t) - F_{tn}\sin\theta_n(t) \tag{28a}$$

$$m_{ry}\ddot{\xi}_r + c_{ry}\dot{\xi}_r + k_{ry}\xi_r = F_y = \sum_{n=1}^{N} -F_{cn}\sin\theta_n(t) - F_{tn}\cos\theta_n(t) \tag{28b}$$

Since the chip load depends on the total x- and y-displacements, and using a matrix to sum the modal coefficients, we can write (for a 3-mode model):

$$\begin{Bmatrix} F_x \\ F_y \end{Bmatrix} = bK_c(\theta)\begin{bmatrix} 1 & 0 & 1 & 0 & 1 & 0 \\ 0 & 1 & 0 & 1 & 0 & 1 \end{bmatrix}\left[\begin{Bmatrix} \eta_1 \\ \xi_1 \\ \eta_2 \\ \xi_2 \\ \eta_3 \\ \xi_3 \end{Bmatrix}(t) - \begin{Bmatrix} \eta_1 \\ \xi_1 \\ \eta_2 \\ \xi_2 \\ \eta_3 \\ \xi_3 \end{Bmatrix}(t-T)\right] + b\vec{f}_0(\theta) \tag{29}$$

or

$$\begin{Bmatrix} F_x \\ F_y \end{Bmatrix} = bK_c'(\theta)\left[\vec{\eta}(t) - \vec{\eta}(t-T)\right] + b\vec{f}_0(\theta) \tag{30}$$

where $K_c'(\theta)$ is a 2x2R matrix and $\vec{\eta}(t)$ is a 2Rx1 vector of modal coefficients. Then we can assemble Equations 28-30 into a single matrix equation of the form

$$M^*\ddot{\vec{\eta}} + C^*\dot{\vec{\eta}} + K^*\vec{\eta} = bK_c^*(\theta)[\vec{\eta} - \vec{\eta}(t-T)] + b\vec{F}_0, \tag{31}$$

and use the procedures outlined in the previous section.

2.3 Variance of 1/tooth samples in Euler simulation

A simple Euler time-marching scheme (Tlusty 1999) with 720 steps/rev was applied to integrate Equations 1a-1b numerically for a 2-flute tool. The Euler method was chosen because the single, uniform time step makes it simple to keep track of time-delayed displacements. In the simulation, loss of contact between the tool and workpiece (while a flute is within the angular range defined by the radial immersion) due to large amplitude tool vibration is treated; additionally, the instantaneous chip thickness is calculated using the current tool vibration and surfaces left by three previous cutter revolutions. The displacements were sampled periodically at 1 sample/tooth (at the time each tooth exits the cut for a down-milling operation). The statistical variance, σ^2, of the 1/tooth samples of total cutter displacement was calcuated using the last 20 of a total of 40 simulated tool revolutions according to Equation 32, where S is the total number of samples, r_i. More details can be found in Schmitz et al. (2001c).

$$\sigma^2 = \frac{\sum_{i=1}^{S}\left(r_i - r_m^2\right)}{S-1}, \ \text{where} \quad r_m = \frac{\sum_{i=1}^{S} r_i}{S} \tag{32}$$

2.4 Cutting tests

Milling tests were performed with an experimental flexure designed corresponding to the 1-DOF system of Section 2.1.2. 1-DOF tests were performed for the current work because of their simplicity and the availability of equipment. The workpiece was clamped on a monolithic, uni-directional flexure machined from aluminum and instrumented with a single non-contact, eddy current displacement transducer, as shown in Figure 2. A radial immersion of RDOC=0.237 was used to up-mill and down-mill aluminum (7075-T6) test samples over a specified range of speeds and axial depths of cut. A 0.750-inch diameter carbide end mill with a single flute was used; the second flute was ground off to remove any effects due to asymmetry or runout. Feed was held constant at 0.004 in/rev.

The stiffness of the flexure to deflections in the x-direction was measured to be $k = 2.18\times10^6$ N/m. The natural frequency was experimentally determined to be 146.5 Hz and the damping ratio $\xi = 0.0032$, which corresponds to very light damping, typical of a monolithic flexure. In comparison, the values of stiffness in the perpendicular y- and z-directions were more than 20 times greater, as was the stiffness of the tool. The cutting coefficients in the tangential and normal direction were determined from the rate of increase in cutting force as a function of chip load during separate cutting tests on a Kistler Model 9255B rigid dynamometer (Halley, 1999). The estimated values were $K_n = 2.0\times10^8$ N/m^2 and $K_t = 5.5\times10^8$ N/m^2.

The displacement transducer output was anti-alias filtered and sampled (16-bit precision, 12800 samples/sec) with SigLab 20-22a data acquisition hardware connected to a Toshiba Tecra 520 laptop computer. A periodic 1/tooth pulse was obtained

Copyright © 2002 by ASME

Downloaded From: https://proceedings.asmedigitalcollection.asme.org on 06/29/2019 Terms of Use: http://www.asme.org/about-asme/terms-of-use

with the use of a laser tachometer to sense a black-white transition on the rotating tool holder.

3 RESULTS

3.1 Analysis and simulation of 2-DOF cutting

A benchmark 2-DOF case was chosen with the following parameters, which were estimated from modal tests on a 12.7 mm (0.5 inch) diameter, 2-flute, carbide helical end mill with a 106.2 mm overhang (9:1 length/diameter ratio) held in an HSK 63A collet-type tool holder: Natural frequency 922 Hz; Stiffness 1.34×10^6 N/m; Damping ratio 0.011. Specific cutting pressures were: $K_c = 6\times10^8$ N/m2 and $K_t = 2\times10^8$ N/m2. These parameters were held to be the same in both directions.

Spindle speed was varied from 5,000 rpm to 21,000 rpm and axial depth of cut (ADOC) was varied from 0 to 10 mm, and radial imersions of 100% (full slot), 50%, 10%, and 5% were used. The eigenvalues of the discrete map (Equation 24) obtained via TFEA were computed. The behavior of eigenvalues during the transition to instability is shown in Figure 3 (ADOC= 3 mm, 5% radial immersion). As speed is increased from 13,500 to 15,500 rpm, two eigenvalues attain a magnitude greater than unity at a speed near 14,500 rpm. The eigenvalues penetrate the unit circle with complex values. As speed is increased again, stability is regained. In the higher speed range shown, from 18,200 rpm to 20,800 rpm, eigenvalues again penetrate the unit circle, re-entering along the negative real axis. This route, associated with a "flip" bifurcation signifies alternating or period-2 behavior.

In Figure 4 simulation results at different speeds are shown (ADOC= 3 mm, 5% radial immersion). Data from continuous sampling and 1/tooth sampling are shown. The 1/tooth data decay to a single steady value for all stable cuts. For unstable cuts, the behavior of the 1/tooth samples depends on what type of instability has occurred. If the instability corresponds to a complex eigenvalue of the discrete map, the 1/tooth samples trace a rotating trajectory in displacement-velocity state space. If the instability corresponds to a negative real eigenvalue, the 1/tooth data appear to flip back and forth between two values.

In Figures 5 and 6, stability boundaries computed via TFEA are compared to boundaries computed by a frequency-domain method (Altintas and Budak, 1995, one-term Fourier approximation of cutting coefficients), and to contours of the variance of 1/tooth samples (dark regions represent low variance and stable cutting, while light areas indicate high variance and chatter). It is apparent that the three methods agree closely for 100% and 50% radial immersion. At 10% radial immersion, small differences arise between the frequency domain method and the other two results. Particularly at 5% radial immersion the TFEA method predicts the results of simulation very well. It is seen in Figures 5c, 6c, and 6f that spurious data points appear (i.e., small areas of low variance in the unstable regions). This is a consequence of the number of revolutions of data used to calculate the variance – a minimum value was chosen to decrease execution time.

To produce these results, the frequency domain analysis was completed in 10-20 seconds, the TFEA method in about 1-2 minutes, but the time-marching simulation required 1-2 days on a Pentium II 266 MHz PC. Results were computed at 100 rpm speed increments and 0.1 mm increments in ADOC (i.e., on a 160 x 100 data grid). All of the methods were implemented in MATLAB[1] and none of the algorithms was optimized for speed. The size of the TFEA transition matrix $\mathbf{Q}$ is $4E+4\times4E+4$. Typically results are converged when $E = 20\rho$ where ρ is the fraction of time in the cut. So for $\rho = 0.1$, $\mathbf{Q}$ is 12×12 and for $\rho = 0.5$, $\mathbf{Q}$ is 24×24.

3.2 Experimental cutting test results: 1-DOF milling including cutter rotation angle

Raw displacement measurements and 1/tooth samples for several example cases of up-milling (A,B,C,D) are shown in Figure 7. Tests were declared stable if the 1/tooth-sampled position of the tool approached a steady constant value. Cases A and C in Figure 7 are clear examples of stable behavior. Unstable behavior predicted by two complex eigenvalues with a magnitude greater than one in the mathematical model corresponds to a Hopf bifurcation. In such cases chatter vibrations are unsynchronized with tooth passage as shown in example B of Figure 7. When the dominant eigenvalue of the mathematical model is negative and real, a magnitude greater than one predicts a period doubling or flip bifurcation. Experimental evidence confirms this prediction where chatter is a subharmonic of order 2 as shown in case D of Figure 7. Stability results from up-milling tests are summarized in Figure 8, along with theoretical stability boundaries obtained by TFEA.

Raw displacement measurements and 1/tooth samples representing down-milling cases (E,F,G,H) on this graph are shown in Figure 9. Stability results from down-milling tests are superimposed over the appropriate stability predictions obtained via TFEAand shown in Figure 10. The agreement between stability predictions and experimental results is generally very good.

The theoretical predictions made by TFEA agree exactly with the predictions obtained independently by the method of Insperger and Stepan (2001). The qualitative difference between up-milling and down-milling stability boundaries seen in Figures 8 and 10 was predicted by Insperger and Stepan (2001). It is confirmed by TFEA for a larger range of speeds and radial depths of cut in Figure 11. Up-milling and down-

[1] Commercial equipment is identified in order to adequately specify certain procedures. In no case does such identification imply recommendation or endorsement by the National Institute of Standards and Technology, nor does it imply that the equipment identified is necessarily the best available for the purpose.

Copyright © 2002 by ASME

Downloaded From: https://proceedings.asmedigitalcollection.asme.org on 06/29/2019 Terms of Use: http://www.asme.org/about-asme/terms-of-use

milling stability regions become identical for a full slot ($\rho = 0.5$ for a 1-flute tool).

4 DISCUSSION AND CONCLUSIONS

TFEA is a newly developed method that complements frequency-domain stability analysis and time-marching simulation. It is useful especially for efficient stability prediction at low radial immersions. TFEA and time-marching results for the 2-DOF symmetric model of milling show less pronounced additional regions of stablity than were observed in 1-DOF interrupted cutting models and tests.

At moderate and high radial immersions, frequency domain methods remain the most advantageous in terms of time and accuracy. Even in these situations, TFEA and time-marching simulation add insight and qualitative information on tool behavior and surface quality. The variance method used to define stability in simulation is a powerful and flexible method for determining stability in both simulations and experiment.

ACKNOWLEDGEMENTS

Support from the Boeing Company and the NSF (DMII-9900108) is gratefully acknowledged. Dr. Matthew Davies of UNC-Charlotte, Charlotte, NC, and Jeremiah Halley of The Boeing Company, St. Louis, MO, provided significant technical guidance.

REFERENCES

Altintas, Y. and Budak, E., 1995, “Analytical prediction of stability lobes in milling,” CIRP Annals, Vol. 44, No. 1, pp. 357-362.

Bayly, P.V., Halley, J.E., Mann, B.P. and Davies, M.A., 2001, “Stability of interrupted cutting by temporal finite element analysis,” Proceedings of ASME Design Engineering Technical Conference, DETC/2001 VIB-21581, Pittsburgh, PA.

Corpus, W.T., and Endres, W.J., 2000, “A high-order solution for the added stability lobes in intermittent machining,” MED-Vol. 11, Proceedings of the ASME Manufacturing Engineering Division, pp. 871-878.

Davies, M.A., Pratt, J.R., Dutterer, B. and Burns, T.J., 2000, “The stability of low radial immersion machining”, CIRP Annals, Vol. 49, pp. 37-40.

Davies, M.A., Pratt, J.R., Dutterer, B., and Burns, T.J., 2001, "Interrupted machining: A doubling in the number of stability lobes, Part 1: Theoretical development", Journal of Manufacturing Science and Engineering, in press.

Halley, J.E., “Stability of low radial immersion milling,” M.S. Thesis, Washington University, 1999.

Insperger, T. and Stépan, G., 2000, “Stability of the milling process,” Periodica Polytechnica Ser. Mech. Eng., Vol. 44, No. 1, pp. 47-57.

Insperger, T., Stepan, G., “Comparison of the stability lobes for up- and down-milling,” Proceedings of Dynamics and Control of Mechanical Processing 2nd Workshop, 2001, Budapest, Budapest University of Technology and Economics, pp. 53-57.

Minis, I. and Yanushevsky, R., 1993, “A new theoretical approach for the prediction of machine tool chatter in milling,” Journal of Engineering for Industry, Vol.115, pp.1-8.

Hou, L.-J., and Peters, D.A., 1994, “Application of triangular space-time finite elements to problems of wave propagation,” Journal of Sound and Vibration, Vol. 173, No. 5, 611-632.

Schmitz, T.L., Ziegert, J., 1999, “Examination of surface location error due to phasing of cutter vibrations,” Precision Engineering Vol. 23, pp. 51-62.

Schmitz, T., Davies, M., Medicus, K., Snyder, J. “Improving high-speed machining material removal rates by rapid dynamic analysis”, Annals of the CIRP, 50(1), 2001a, pp. 263-268.

Schmitz, T.L., 2001b, “Chatter recognition by a statistical evaluation of the synchronously sampled audio signal”, Proceedings of the 2001 India-USA Symposium on Emerging Trends in Vibration and Noise Engineering, Columbus, OH, December 10-14.

Schmitz, T.L., Medicus, K., Dutterer, B., 2001c, “Exploring once-per-revolution audio signal variance as a chatter indicator”, Machining Science and Technology, in press.

Tlusty, J., Polacek, A., Danek, C., Spacek, J.: Selbsterregte Schwingungen and Werkzuegmaschinen, VEG Verlag Technik, Berlin, 1962.

J. Tlusty, 1999, Manufacturing Processes and Equipment, Prentice Hall, Upper Saddle River, NJ.

Tobias, S.A, 1965, Machine Tool Vibration, Wiley, New York.

Copyright © 2002 by ASME

Downloaded From: https://proceedings.asmedigitalcollection.asme.org on 06/29/2019 Terms of Use: http://www.asme.org/about-asme/terms-of-use

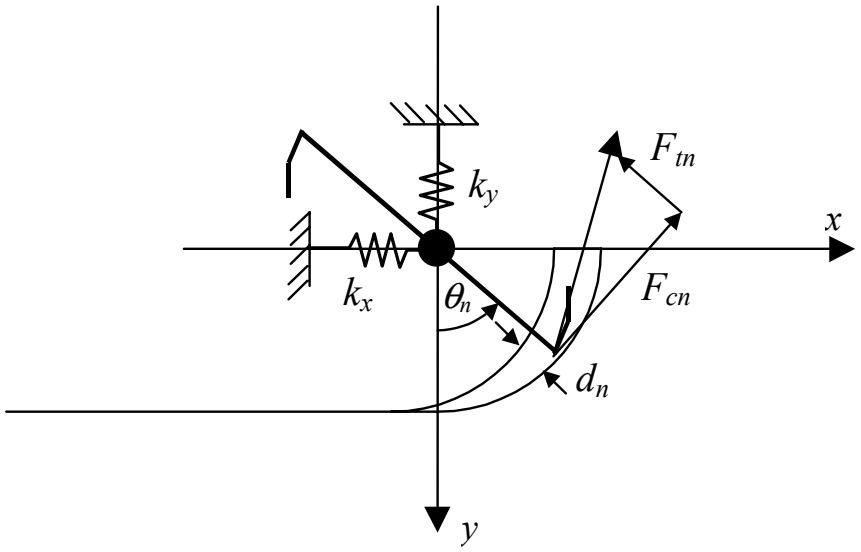

Figure 1: A 2-DOF model of milling. Fraction of time in the cut is determined by the radial immersion (radial depth of cut/tool diameter) and number of teeth. The angle θ decreases with tool rotation.

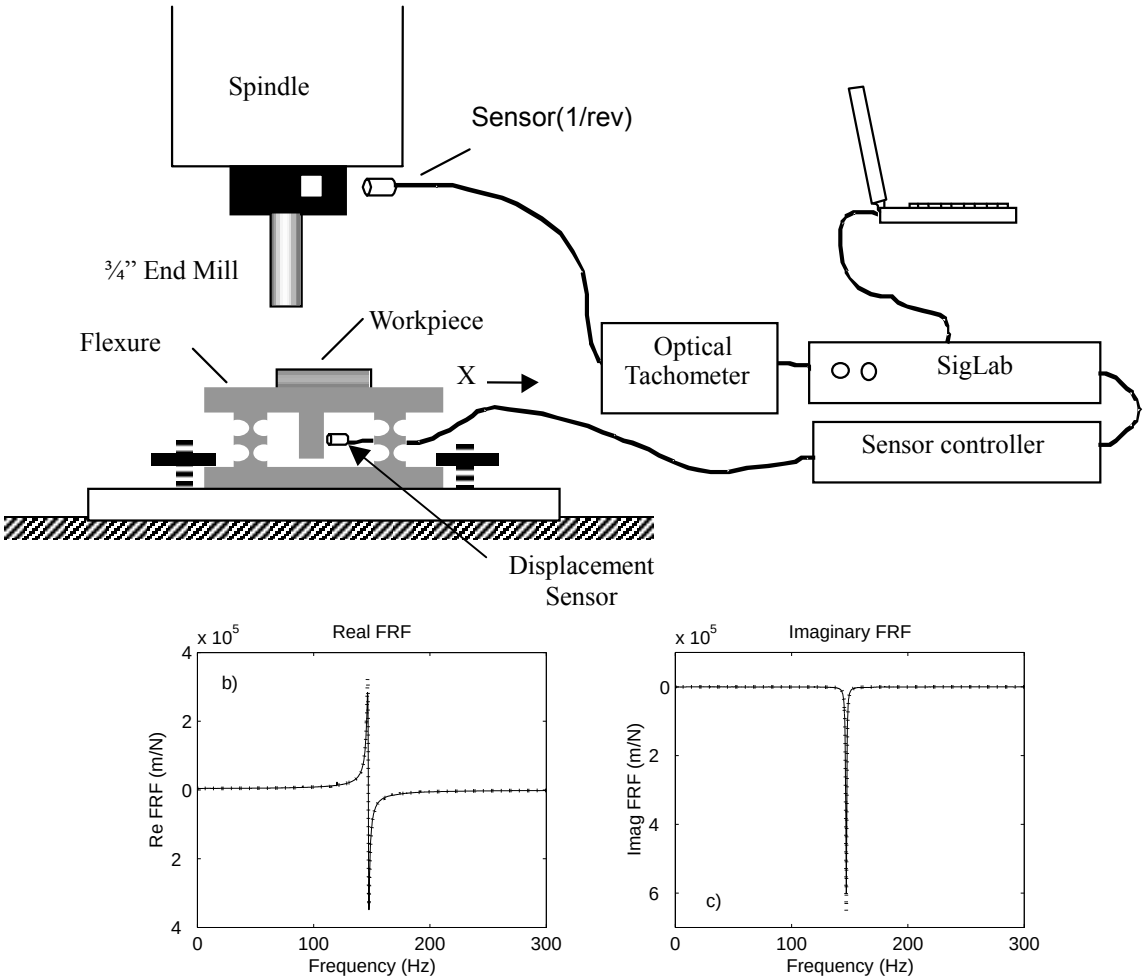

Figure 2: (a) Schematic diagram of the 1-DOF experiment. (b-c) Frequency response function of the flexure. Fitted parameters are: $k = 2.18 \times 10^6$ N/m; f_n=146.5 Hz ; damping ratio $\xi = 0.0032$, Damping is extremely light in the monolithic aluminum structure.

Copyright © 2002 by ASME

Downloaded From: https://proceedings.asmedigitalcollection.asme.org on 06/29/2019 Terms of Use: http://www.asme.org/about-asme/terms-of-use

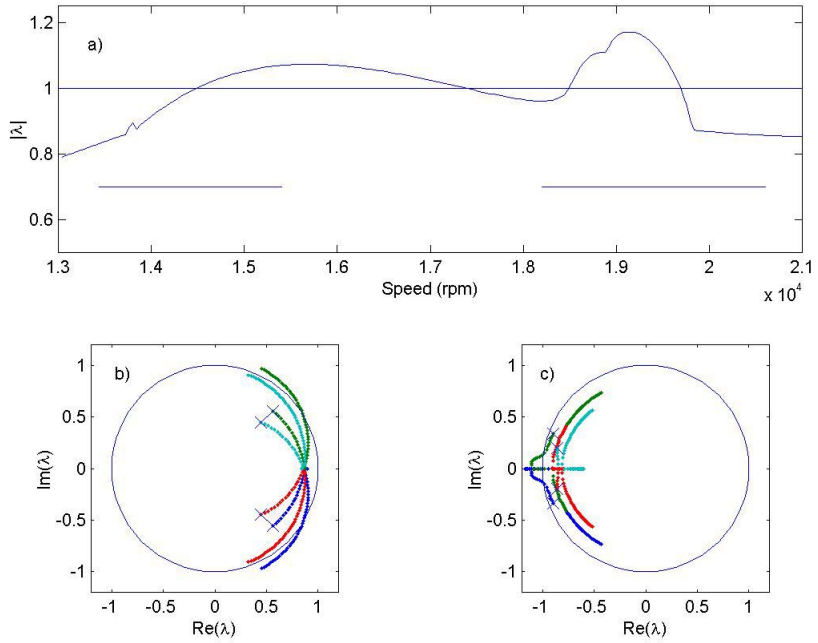

Figure 3: 2-DOF. Eigenvalue (λ) behavior of discrete map from TFEA of 2-DOF model as speed is increased. ADOC 3 mm. 5% radial immersion. (a) Magnitude vs speed, showing two instability regions where $|\lambda|>1$. (b) Eigenvalue trajectory in complex plane in first region of instability (Hopf bifurcation); (c) Eigenvalue trajectory in second region of instability (flip bifurcation).

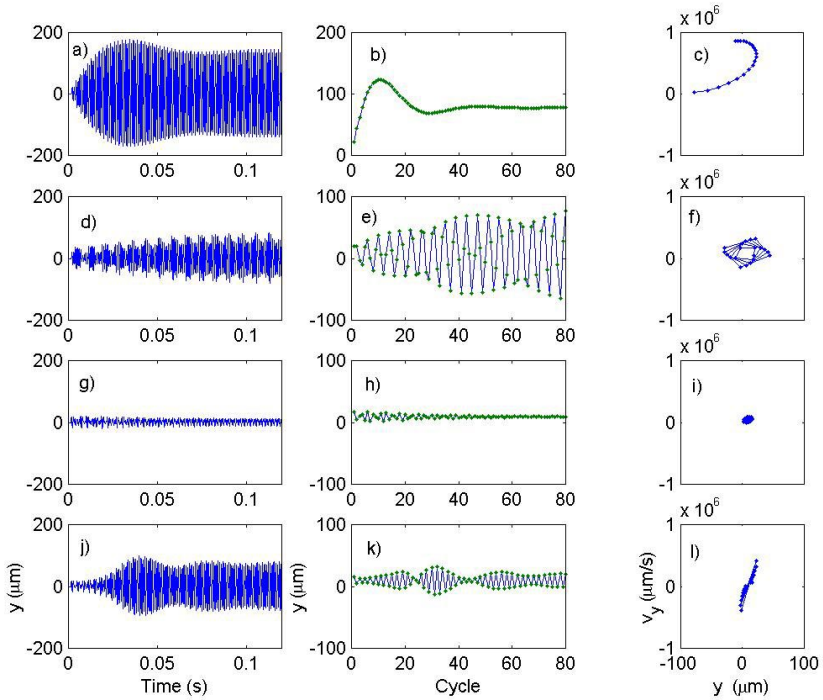

Figure 4: 2-DOF. Output from 2-DOF simulation showing time series of y-displacement, 1/tooth samples of y-displacement, and 1/tooth plots of y-displacement vs y-velocity. ADOC = 3 mm. 5% radial immersion. (a-c) 14000 rpm (stable, variance = 65 μm^2); (d-f) 16000 rpm (unstable, variance = 973 μm^2); (g-i) 18000 rpm (stable, variance = 28 μm^2); (j-l) 19000 rpm (unstable, variance = 403 μm^2).

Copyright © 2002 by ASME

Downloaded From: https://proceedings.asmedigitalcollection.asme.org on 06/29/2019 Terms of Use: http://www.asme.org/about-asme/terms-of-use

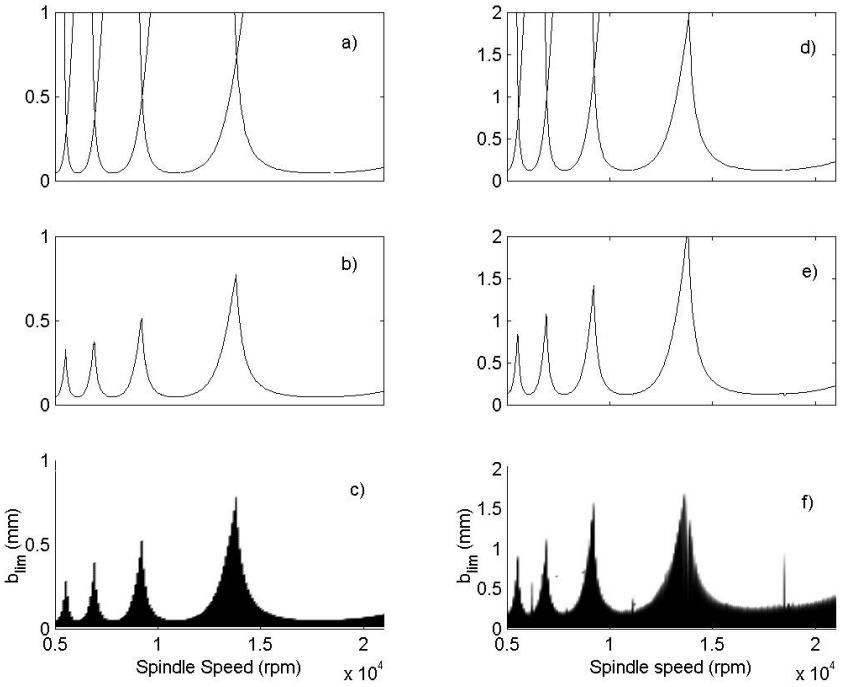

Figure 5: 2-DOF: Stability lobes for 2-DOF model (limiting depth of cut vs spindle speed) obtained via (a,d) frequency domain analysis, (b,e) TFEA, and (c,f) variance of 1/tooth samples from time-marching simulation. (a-c) 100% radial immersion; (d-f) 50% radial immersion.

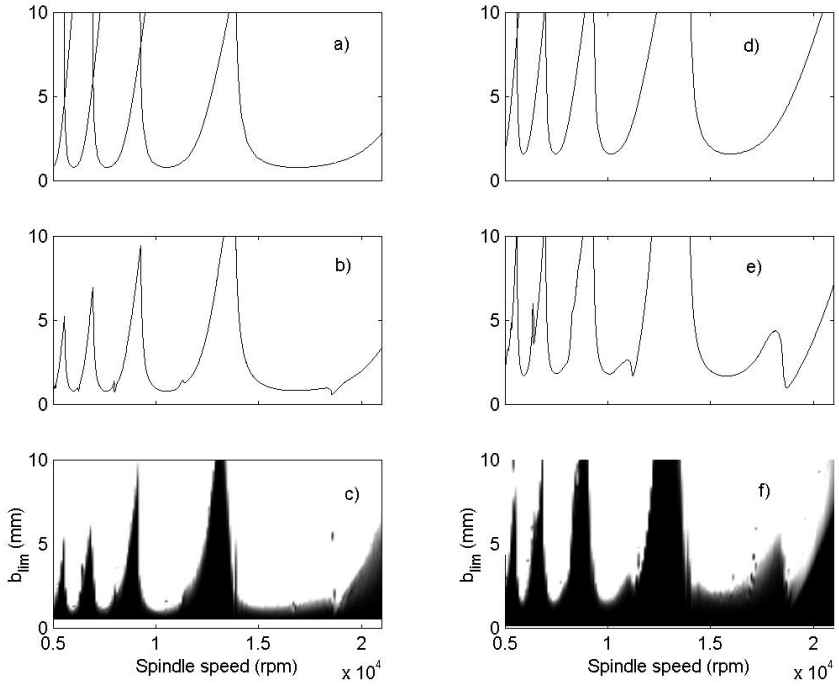

Figure 6: 2-DOF: Stability lobes for 2-DOF model obtained via (a,d) frequency domain analysis, (b,e) TFEA, and (c,f) variance of 1/tooth samples from time-marching simulation. (a-c) 10% radial immersion; (d-f) 5% radial immersion.

Copyright © 2002 by ASME

Downloaded From: https://proceedings.asmedigitalcollection.asme.org on 06/29/2019 Terms of Use: http://www.asme.org/about-asme/terms-of-use

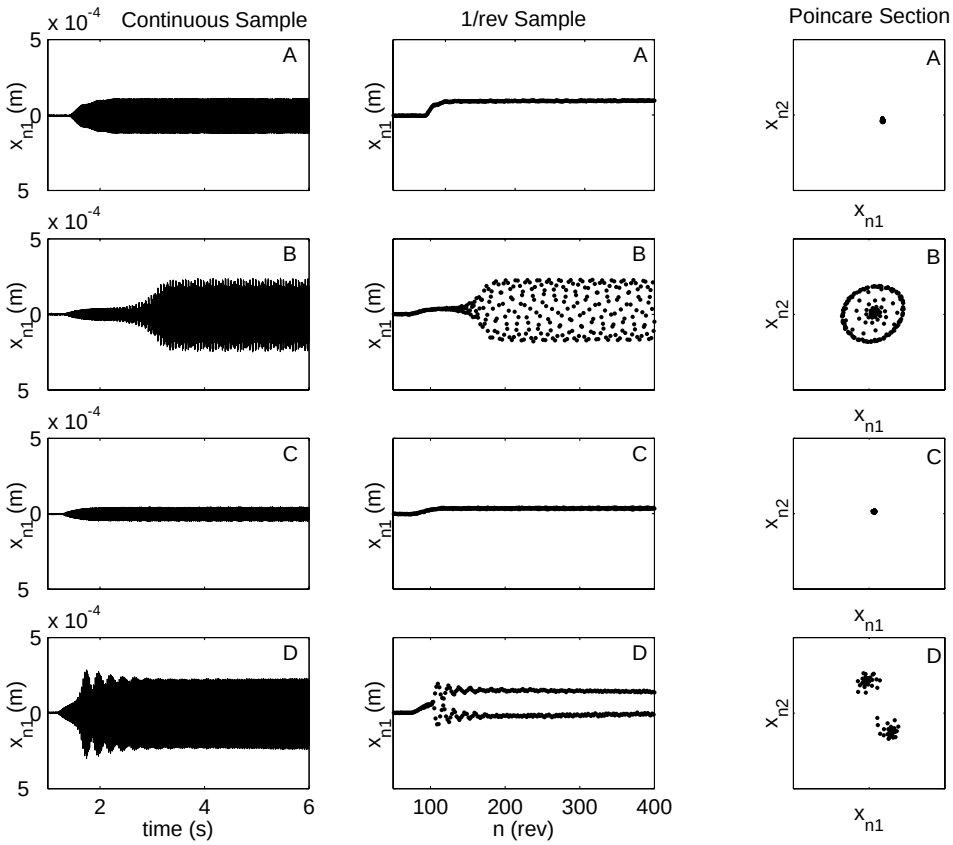

Figure 7: 1-DOF: Up-milling experimental data for cases (A,B,C,D) of Figure 8. Each row contains a continuous sampling plot, a 1/tooth plot, and a Poincare section shown in delayed coordinates. Plots for cases A (RPM=3000, b=0.5mm) and C (RPM=3550, b=1.1mm) are stable. Case B (RPM=3300, b=0.8mm) is a Hopf bifurcation and case D (RPM=3650, b=2.3mm) is a flip bifurcation.

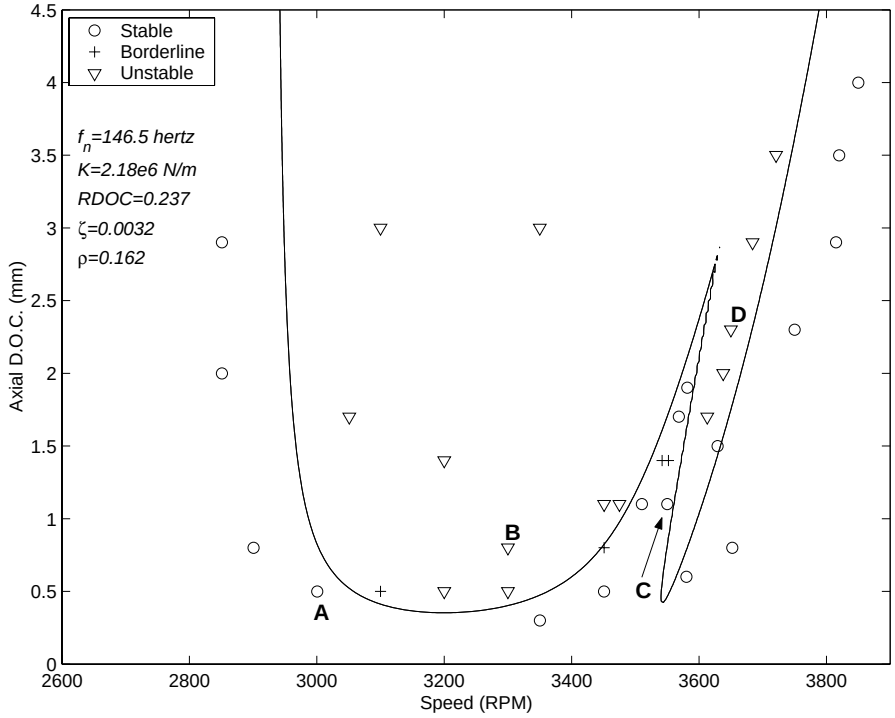

Figure 8: 1-DOF: Summary of 1-DOF up-milling experimental results and stability boundaries predicted by TFEA.

Copyright © 2002 by ASME

Downloaded From: https://proceedings.asmedigitalcollection.asme.org on 06/29/2019 Terms of Use: http://www.asme.org/about-asme/terms-of-use

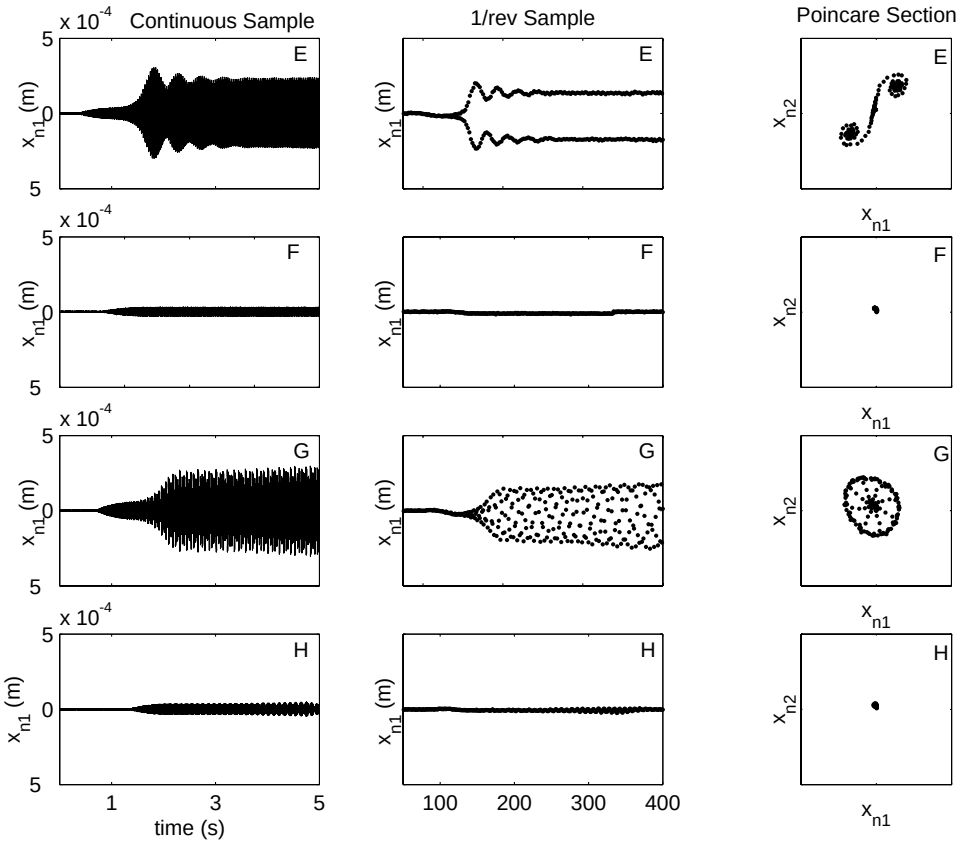

Figure 9: 1-DOF: Down-milling experimental data for cases (E,F,G,H) of Figure 10. Each row contains a continuous sampling plot, a 1/tooth plot, and a Poincare section shown in delayed coordinates. Plots for cases F (RPM=3550, b=1.1mm) and H (RPM=4106, b=0.5mm) are stable. Case G (RPM=3600, b=2.1mm) is a Hopf bifurcation and case E (RPM=3457, b=1.3mm) is a flip bifurcation.

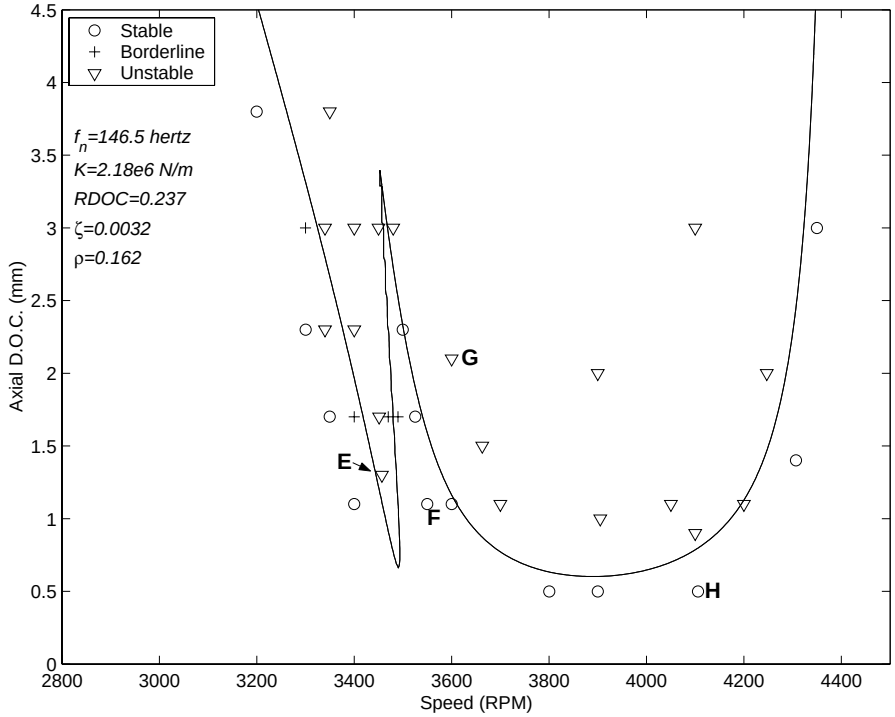

Figure 10: 1-DOF: Summary of 1-DOF down-milling experimental results vs stability predictions obtained by TFEA.

Copyright © 2002 by ASME

Downloaded From: https://proceedings.asmedigitalcollection.asme.org on 06/29/2019 Terms of Use: http://www.asme.org/about-asme/terms-of-use

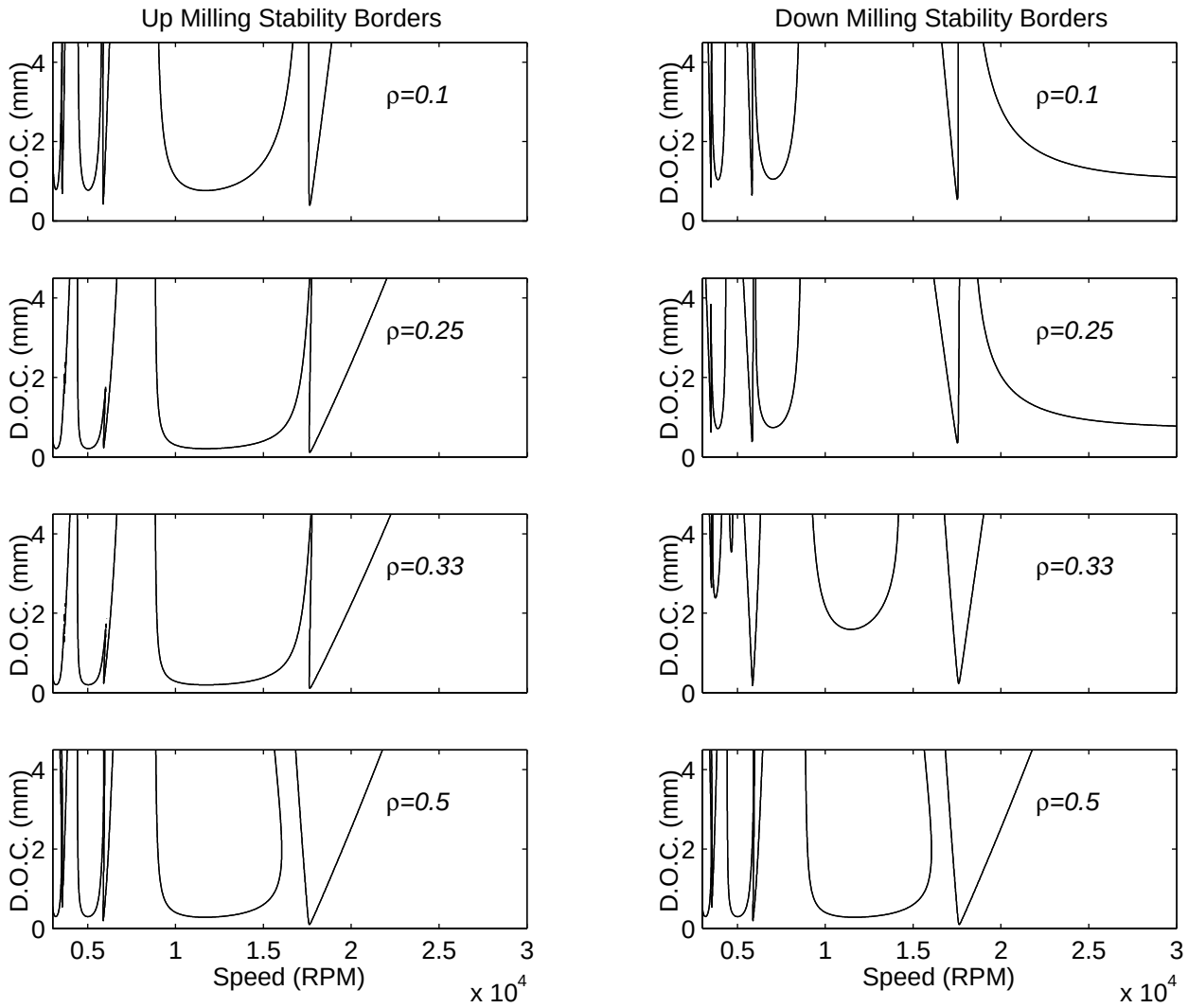

Figure 11: 1-DOF: Comparison of up-milling and down-milling stability boundaries predicted by TFEA for a single flute tool and a 1-DOF flexible workpiece, incorporating cutter rotation angle. The boundaries are quite different at low radial immersion due to the different angle of the cutting force. In a full slot, $\rho = 0.5$, up-milling and down-milling are identical. Note that fraction of time in the cut $\rho = 0.5$ in a full slot since there is only one tooth.

Copyright © 2002 by ASME

Downloaded From: https://proceedings.asmedigitalcollection.asme.org on 06/29/2019 Terms of Use: http://www.asme.org/about-asme/terms-of-use